Synthesis of heterobimetallic gold(I) ferrocenyl-substituted 1,2,3-triazol-5-ylidene complexes as potential anticancer agents

Electronic Supplementary Information

Danielle Aucamp,[a],[b] Sreedhar V. Kumar,[a] David C. Liles,[b] Manuel A. Fernandes,[a] Leonie Harmse[c] and Daniela I. Bezuidenhout*[a]

[a] Molecular Sciences Institute, School of Chemistry, University of the Witwatersrand, Johannesburg 2050, South Africa

[b] Chemistry Department, University of Pretoria, Private Bag X20, Hatfield 0028, Pretoria, South Africa

[c] Division of Pharmacology, Department of Pharmacy and Pharmacology, Faculty of Health Sciences, University of the Witwatersrand, 7 York Road, Parktown, 2193, South Africa.

Email: daniela.bezuidenhout@wits.ac.za

Table of Contents

I. General considerations

Nuclear magnetic resonance (NMR) spectra were obtained using either a Bruker AVANCE-III-300 operating at 300.13 MHz for ^{1}H, 75.47 MHz for ^{13}C, 121.49 MHz for ^{31}P and 282.40 MHz for ^{19}F; or AVANCE-III-400 operating at 400.21 MHz for ^{1}H, 100.64 MHz for ^{13}C, 162.01 MHz for ^{31}P and 376.57 MHz for ^{19}F. ^{1}H Chemical shifts are reported as δ (ppm) values downfield from Me_4Si and chemical shifts were referenced to residual non-deuterated solvents peaks ($CDCl_3$, 7.26 ppm). $^{13}C\{^{1}H\}$ chemical shifts are also reported as δ (ppm) values downfield from Me_4Si and chemical shifts were referenced to residual non-deuterated solvents peaks ($CDCl_3$, 77.16 ppm). The chemical shifts are given in ppm and the proton coupling constants (*J*) are given in Hz. The spectral coupling patterns are designated as follows: s - singlet; d - doublet; t - triplet; q - quartet; sept-septet; m - multiplet; br - broad signal. The assignment of the

NMR for each complex follows the numbering scheme individually assigned for each compound illustrated on the respective NMR spectra below. An asterisk (*) denotes solvent contaminant in the NMR spectra. Chemical shift assignment in the ^{1}H NMR spectra is based on first-order analysis and when required were confirmed by two-dimensional (2D) (^{1}H-^{1}H) homonuclear chemical shift correlation (COSY) experiments. The ^{13}C shifts were obtained from proton-decoupled ^{13}C NMR spectra. Where necessary, the multiplicities of the ^{13}C signals were deduced from proton-decoupled DEPT-135 spectra. The resonances of the proton-bearing carbon atoms were correlated with specific proton resonances using 2D (^{13}C-^{1}H) heteronuclear single-quantum coherence (HSQC) experiments. Standard Bruker pulse programs were used in the experiments. Single crystal X-ray diffraction data were collected on a Bruker D8 Venture with Apex3 and a Photon 100 CMOS detector (**2** – **5**) or a Bruker Apex II with a CCD detector (**6**) using Mo-K_{α} radiation (λ = 0.71073 Å) (*Iμs*, **2** – **5**; sealed tube, **6**). Crystals were selected under paratone oil, mounted on nylon loops then immediately placed in a cold stream of N_2 at 150 K (at 173 K for **6**). Data were reduced using Bruker SAINT and SADABS, solved using Bruker SHELXTS and refined using SHELXTL (**2** – **5**) and Olex2 (**6**).[1] Mass spectral analyses were performed on a Waters Synapt G2 HDMS by direct infusion at *5* μL/min with positive electron spray as the ionization technique. The *m/z* values were measured in the range of 400-1500 with acetonitrile as solvent. Prior to analysis, a 5 mM sodium formate solution was used to calibrate the instrument in resolution mode. Elemental analyses were carried out using a Thermo Flash 1112 Series CHNS-O Analyzer.

II. NMR Spectra of complexes **1**–**6**

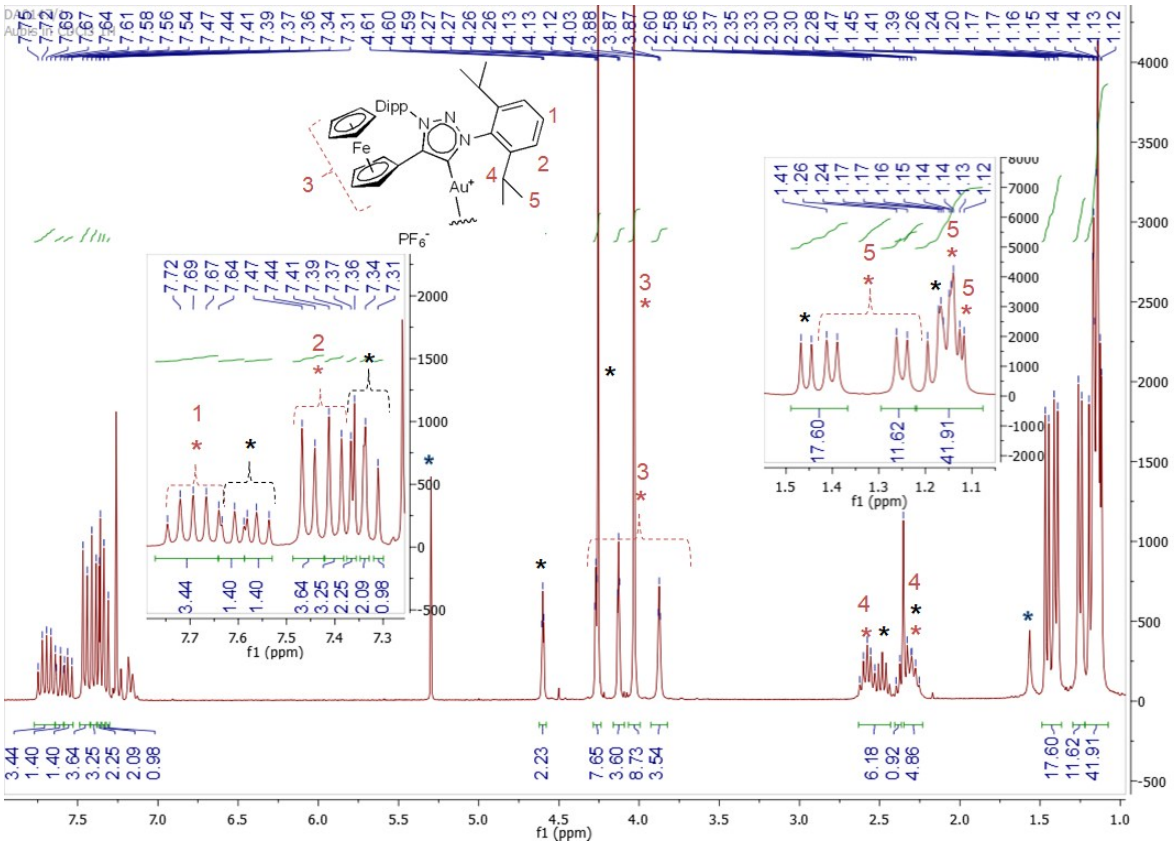

Figure **S1**. The ^{1}H NMR spectrum showing the presence of two gold(I) complexes, where (*) denotes the peaks belonging to the cationic biscarbene gold(I) complex (**1**), and (*****) denotes neutral complex **2** in solvent $CDCl_3$.

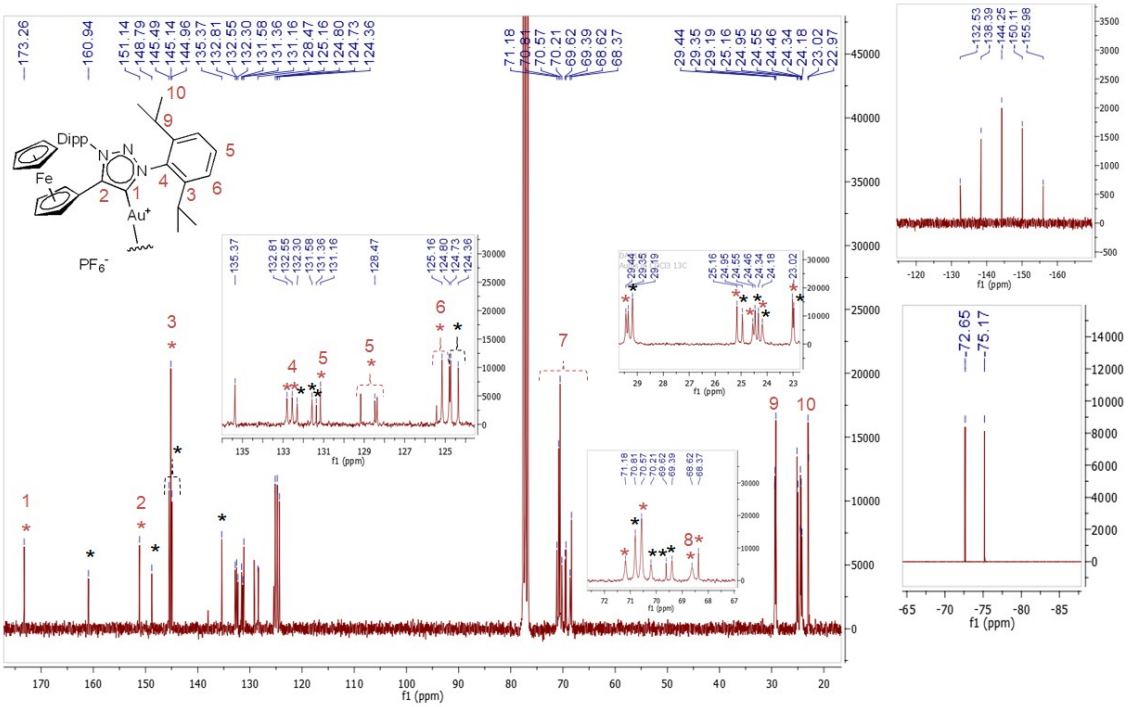

Figure **S2**. The ^{13}C NMR spectrum showing the presence of two gold(I) complexes, where (*) denotes the peaks belonging to the cationic biscarbene gold(I) complex (**1**) and (*) denotes complex **2** in solvent $CDCl_3$. The ^{31}P NMR spectrum is shown top right, and the ^{19}F NMR spectrum bottom right.

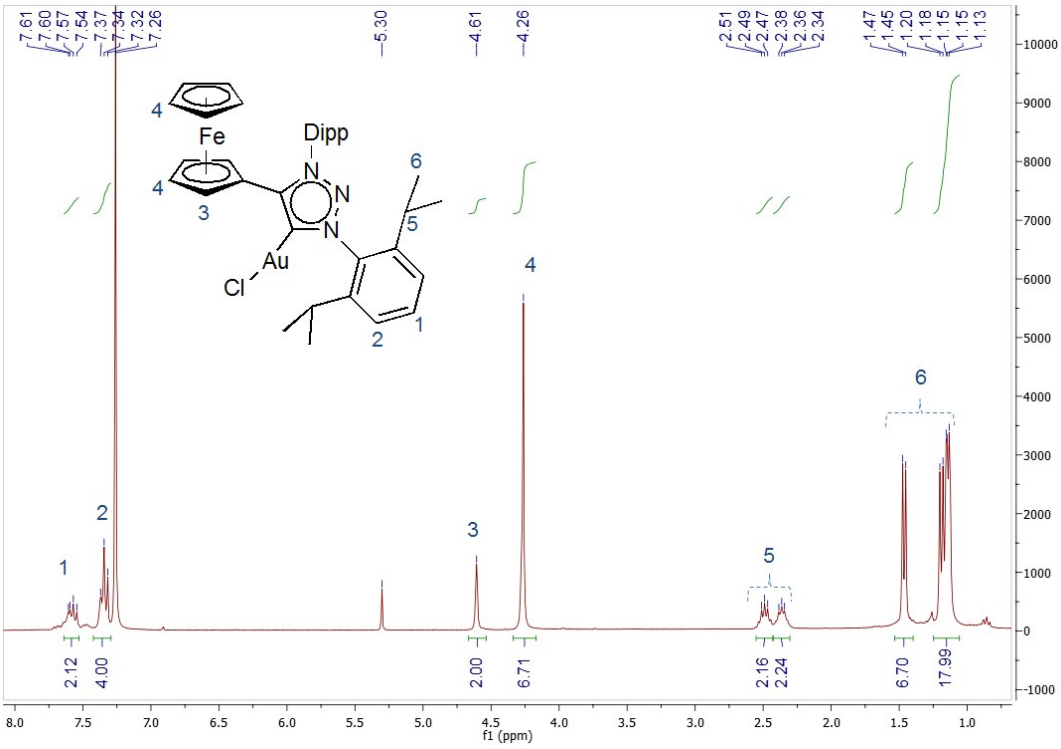

Figure **S3**. The ^{1}H NMR spectrum of the triazolylidene chlorido gold(I) complex **2** in solvent $CDCl_3$.

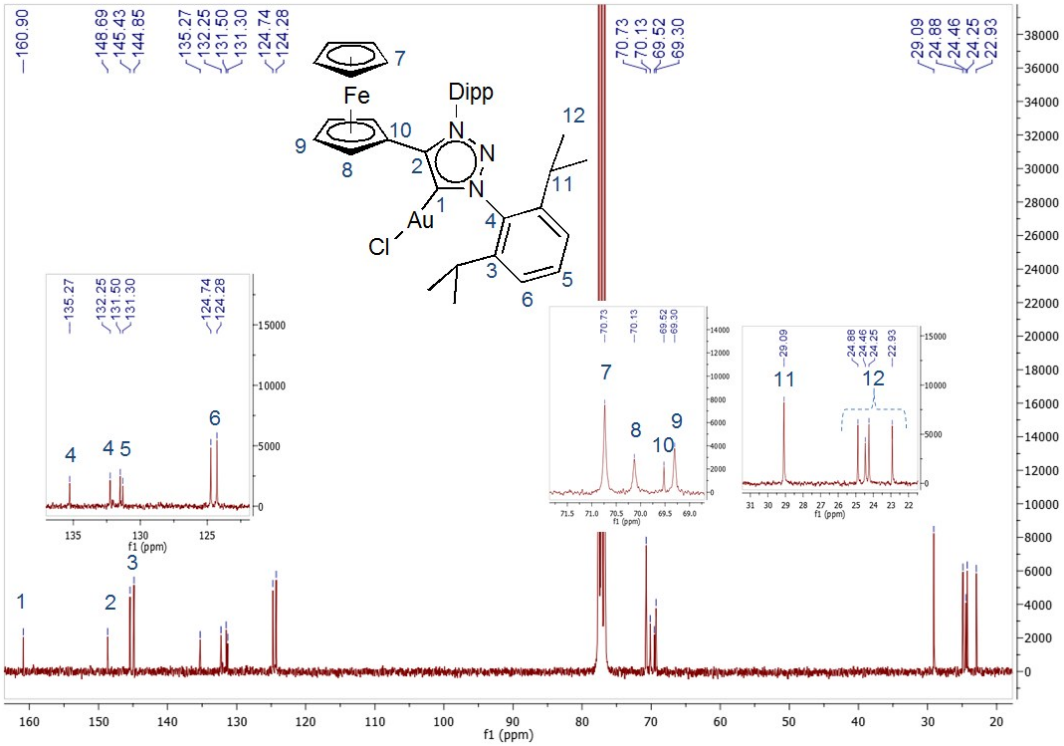

Figure **S4**. The ^{13}C NMR spectrum of the triazolylidene chlorido gold(I) complex **2** in solvent $CDCl_3$.

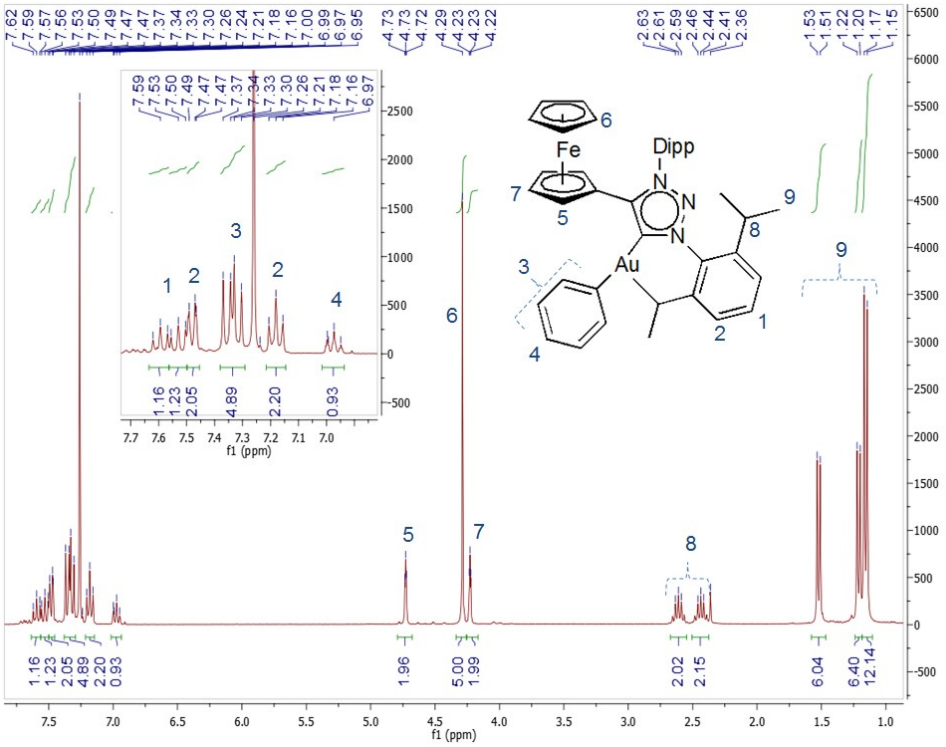

Figure **S5**. The ^{1}H NMR spectrum of the triazolylidene phenyl gold(I) complex **3** in solvent $CDCl_3$.

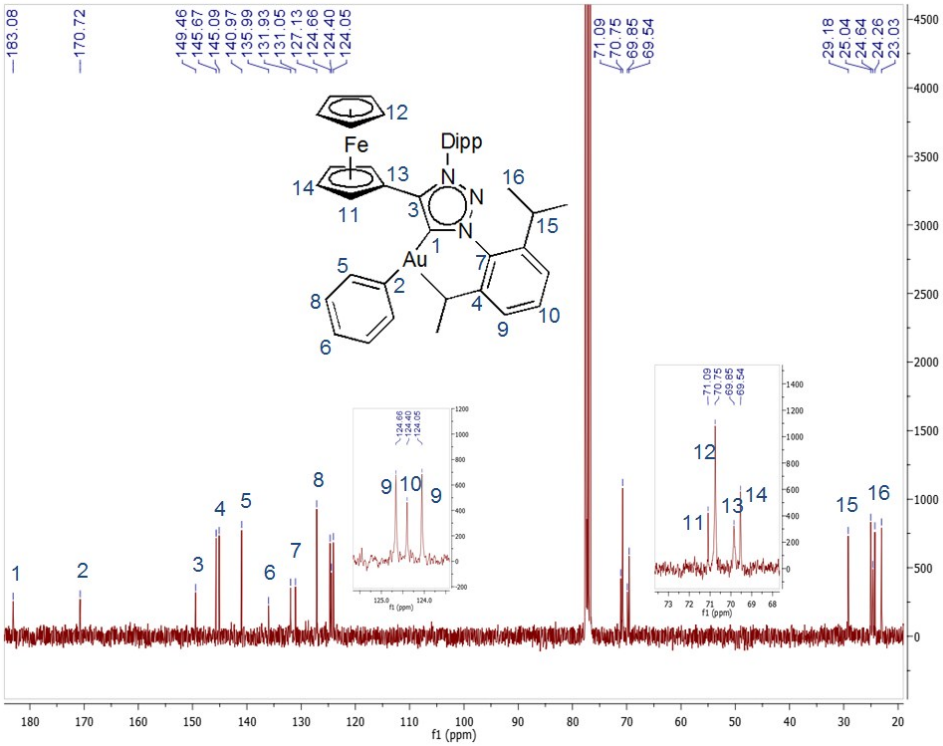

Figure **S6**. The ^{13}C NMR spectrum of the triazolylidene phenyl gold(I) complex **3** in solvent $CDCl_3$.

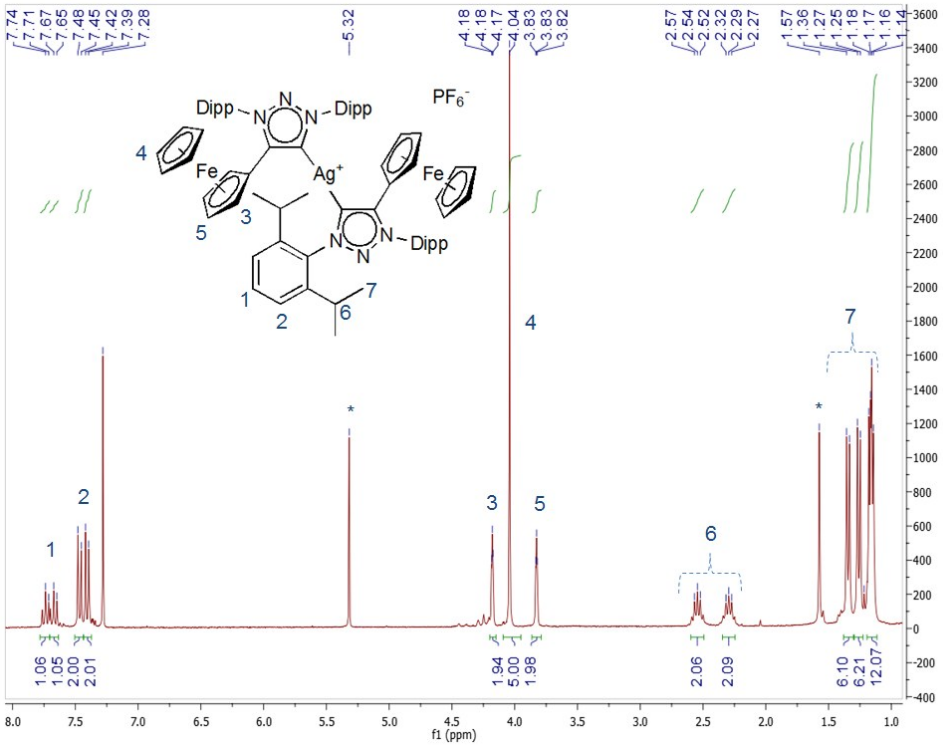

Figure **S7**. The ^{1}H NMR spectrum of the cationic bis(triazolylidene) silver(I) complex **4** in solvent $CDCl_3$.

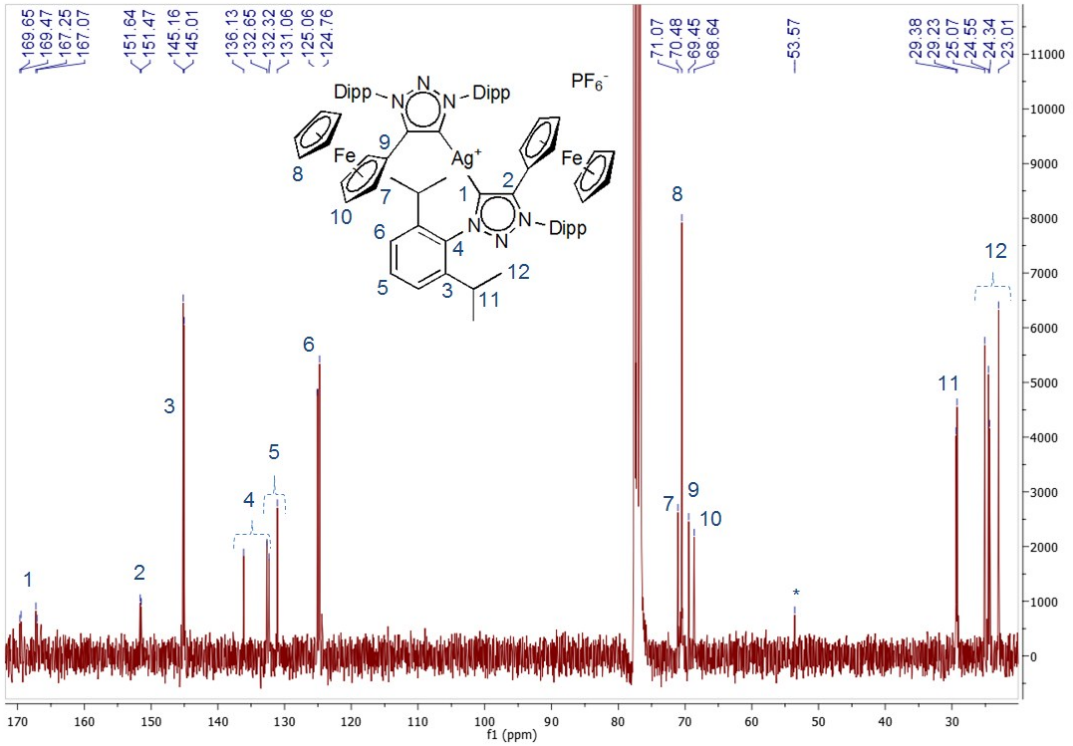

Figure **S8**. The ^{13}C NMR spectrum of the cationic bis(triazolylidene) silver(I) complex **4** in solvent $CDCl_3$.

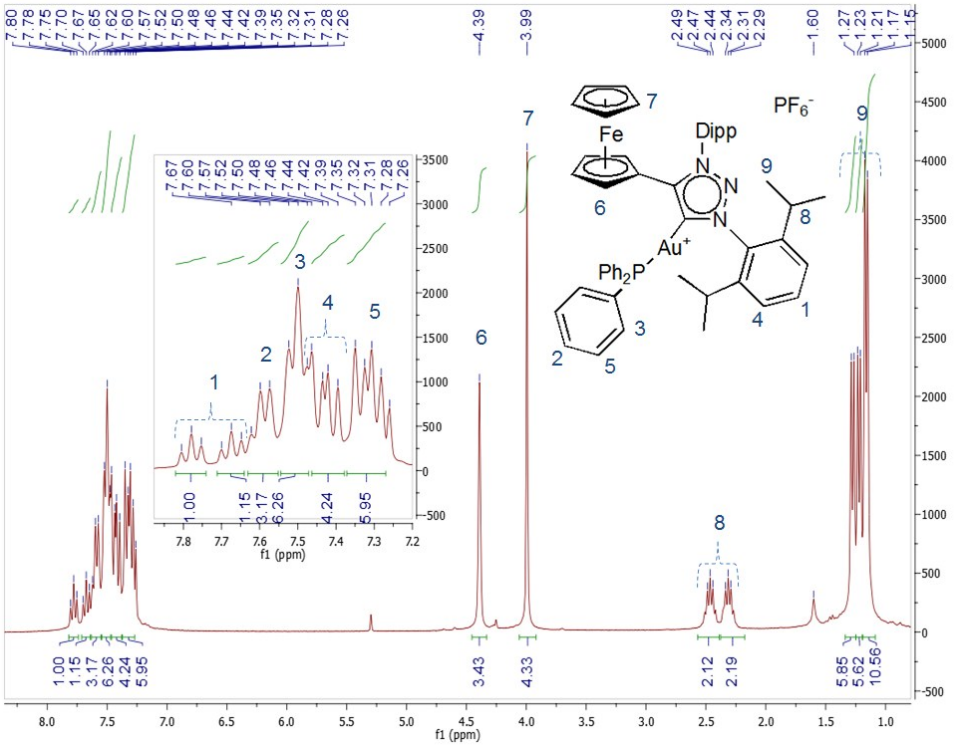

Figure **S9**. The ^{1}H NMR spectrum of the cationic triazolylidene triphenylphosphine gold(I) complex **5** in solvent $CDCl_3$.

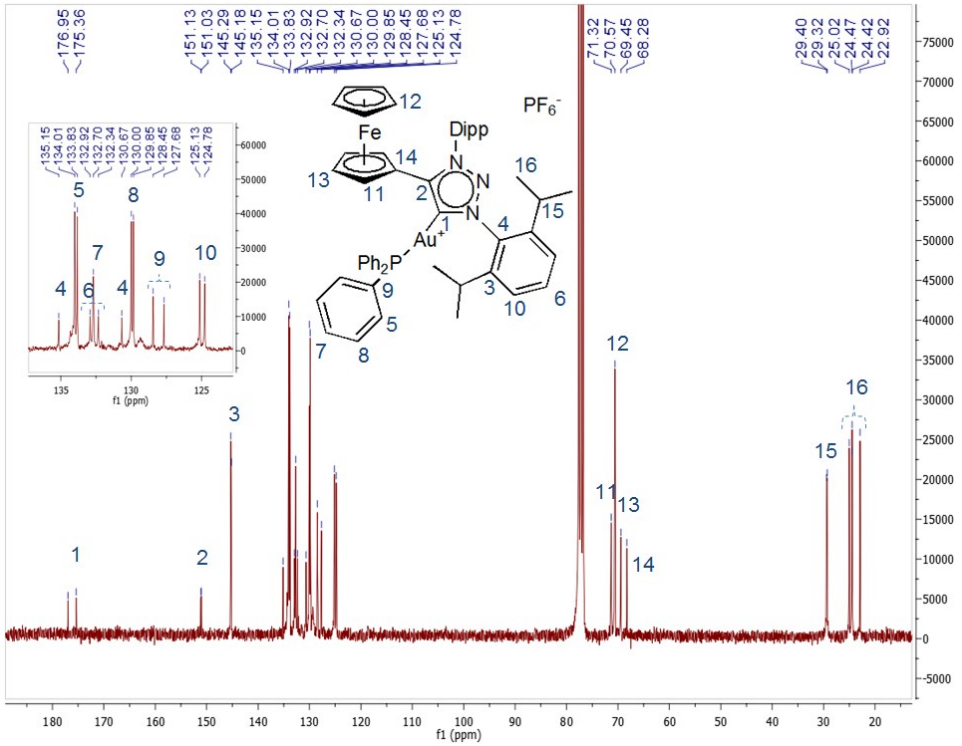

Figure **S10**. The ^{13}C NMR spectrum of the cationic triazolylidene triphenylphosphine gold(I) complex **5** in solvent $CDCl_3$.

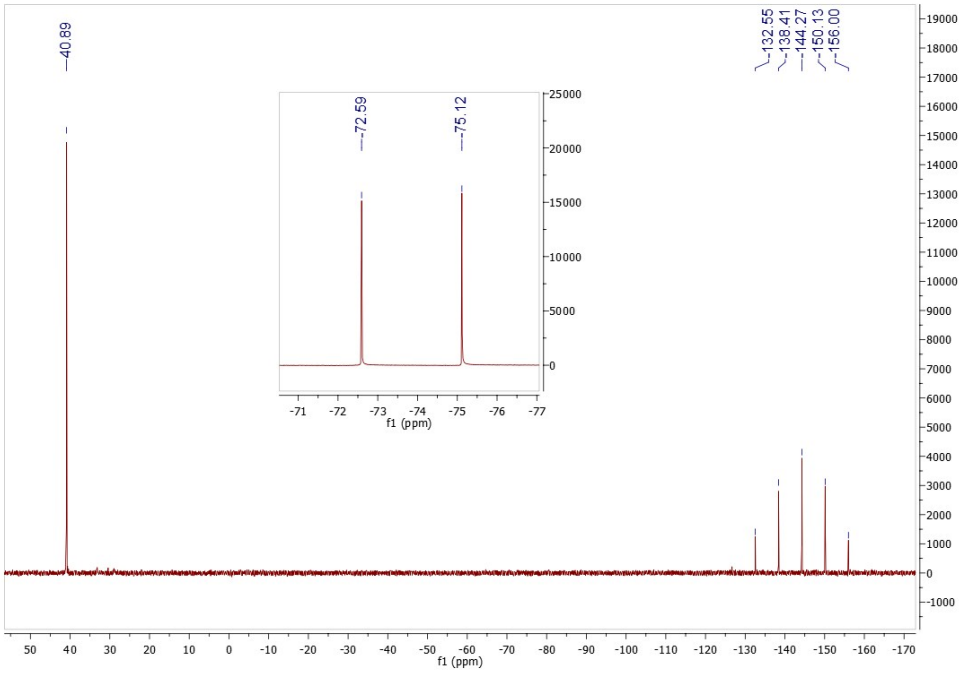

Figure **S11**. The ^{31}P NMR and the ^{19}F NMR (inside block) spectra of cationic triazolylidene triphenylphospine gold(I) complex **5** in solvent $CDCl_3$.

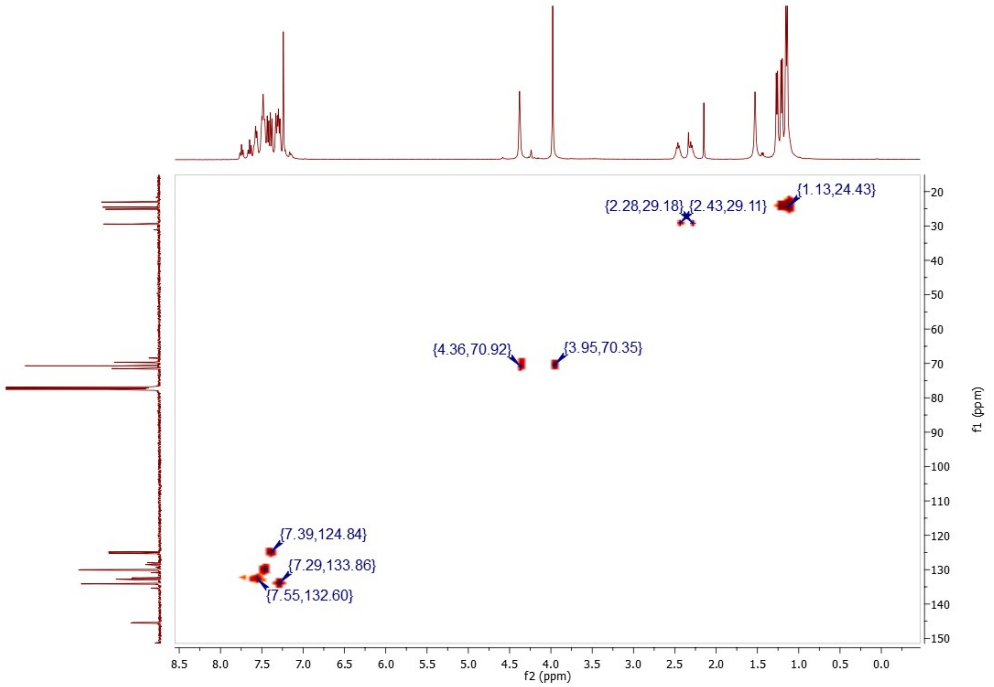

Figure **S12**. The HSQC (2D NMR) spectrum of the cationic triazolylidene triphenylphospine gold(I) complex **5** in solvent $CDCl_3$.

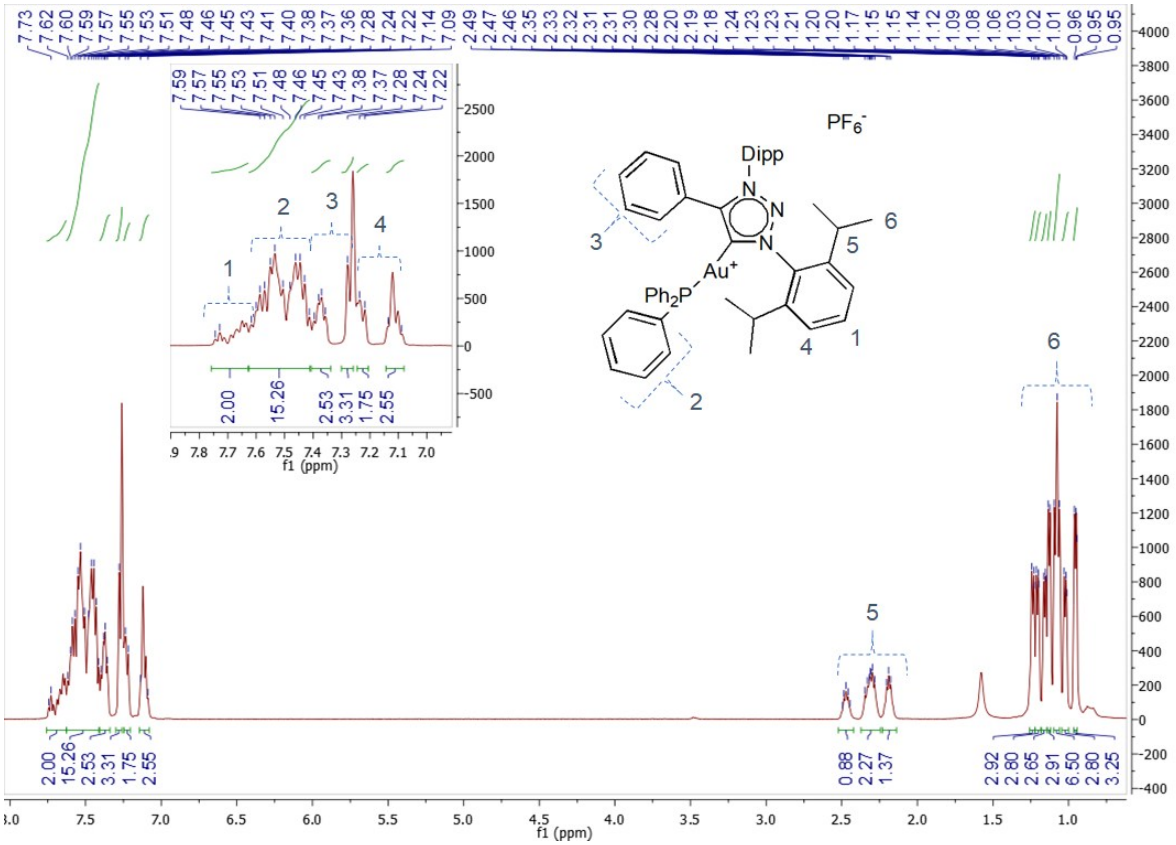

Figure **S13**. The ^1H NMR spectrum of the cationic triazolylidene triphenylphosphine gold(I) complex **6** in solvent $CDCl_3$.

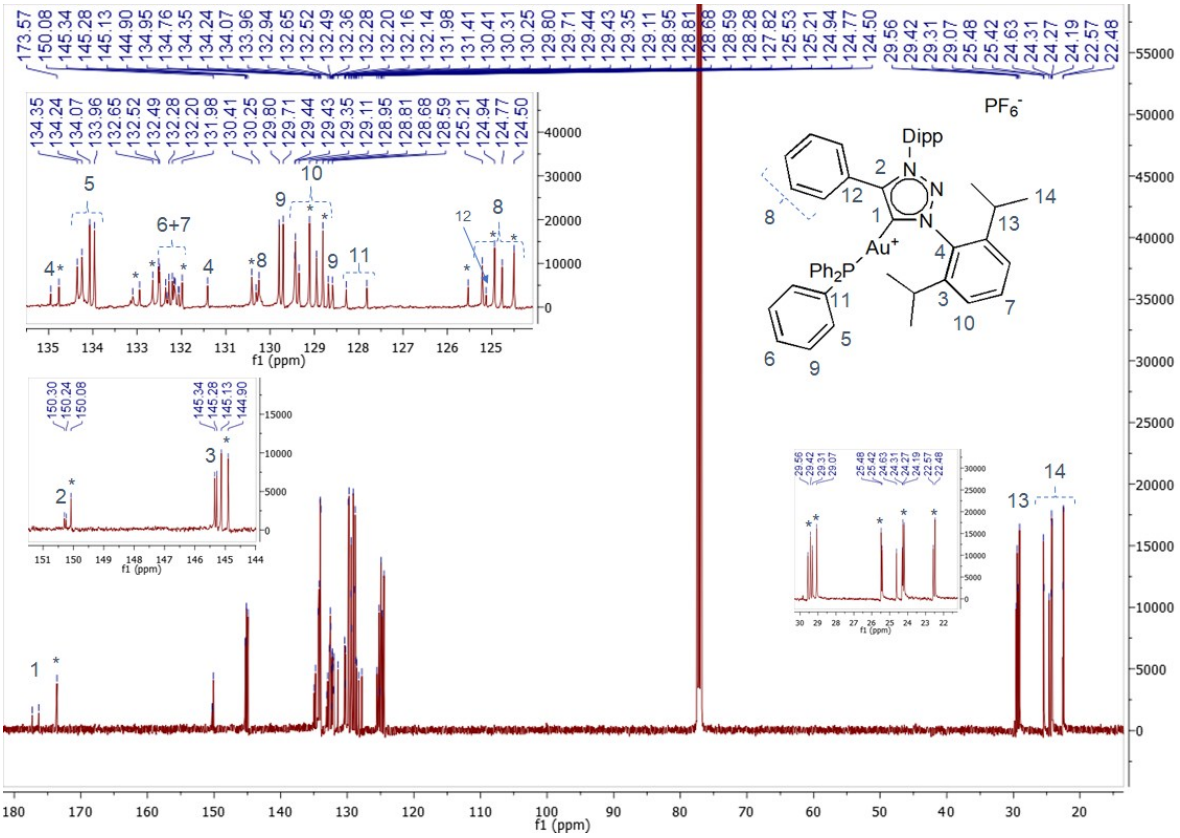

Figure **S14**. The ^{13}C NMR spectrum of the cationic triazolylidene triphenylphosphine gold(I) complex **6** in solvent $CDCl_3$. The set of signals denoted (*) belongs to **bis[(1,3-bis(2,6-diisopropylphenyl)-4-phenyl-1,2,3-triazol-5-ylidene] gold(I) hexafluorophosphate** complex (decomposition product).

III. Cyclic voltammograms of complexes **2** and **5**

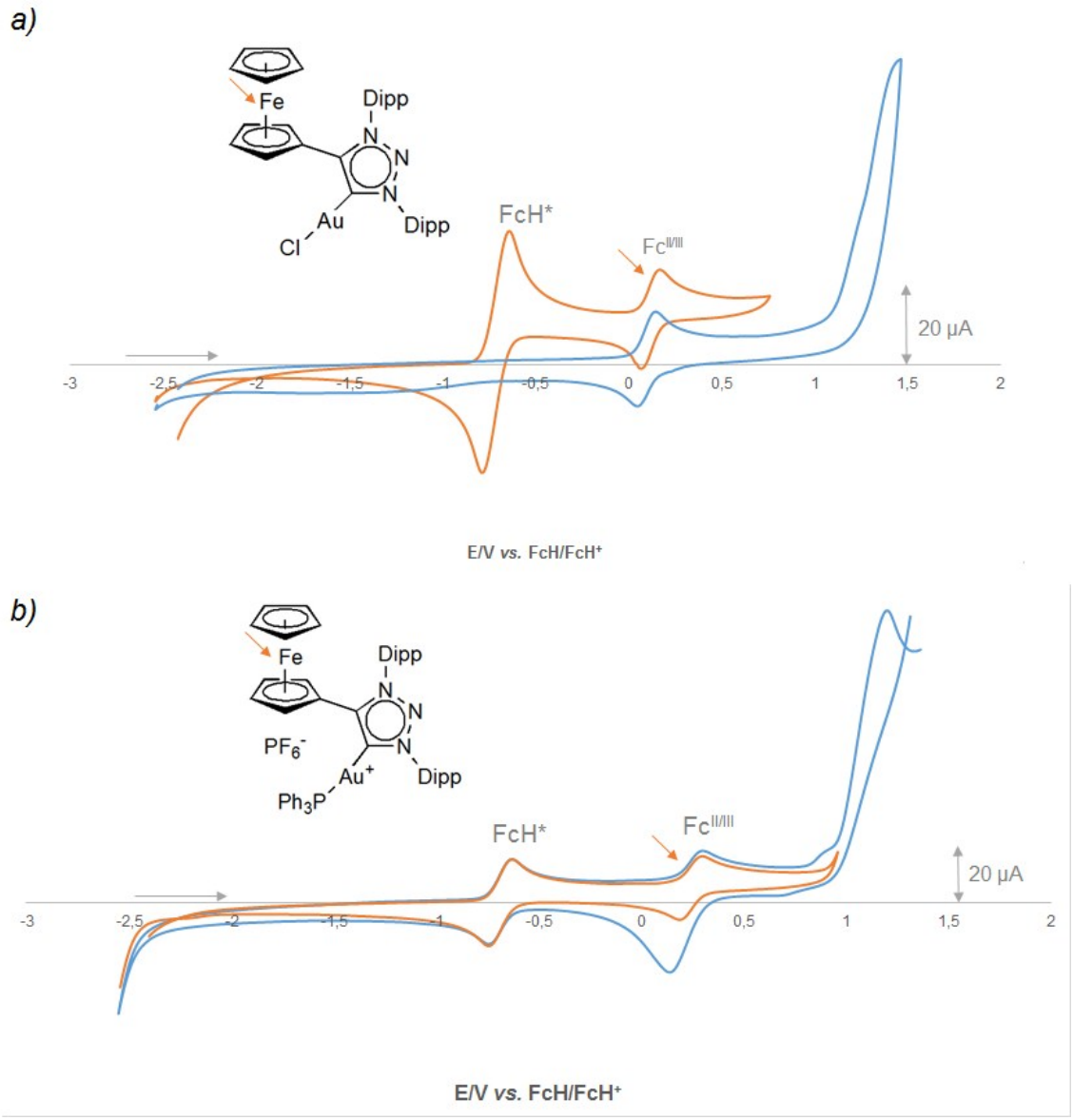

Figure **S15**. The CVs obtained for (a) **2** and (b) **5** at a glassy carbon electrode at a scan rate of 0.1 V. s^{-1} in CH_2Cl_2, with decamethylferrocene (FcH*) as internal standard. In both cases, the curtailed cyclic voltammograms are overlaid in orange.

IV. Stability determination of **2** and **5** in d_6-DMSO by ^{1}H-NMR spectroscopy and mass spectrometry

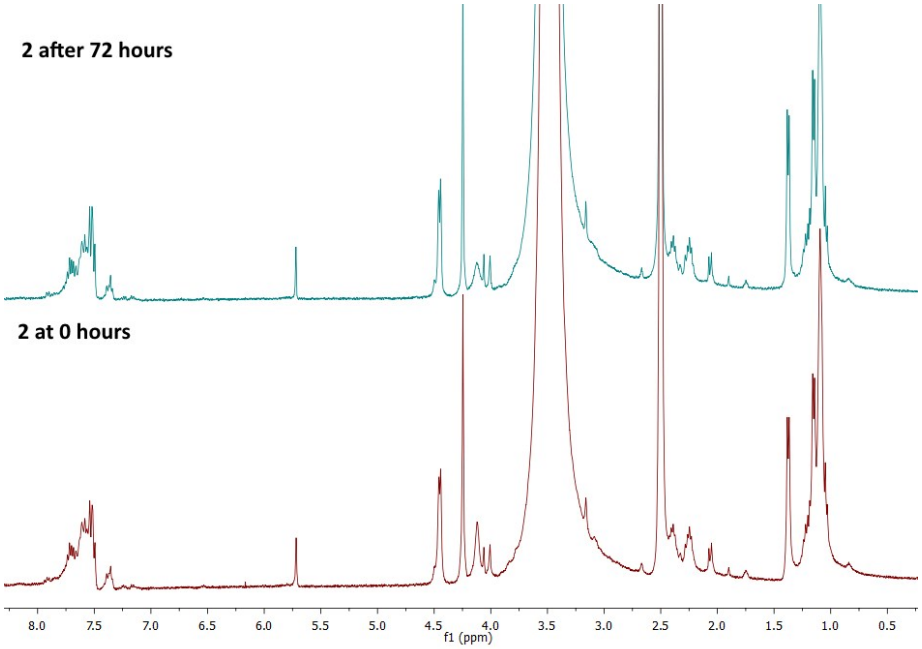

Figure **S16**. ^{1}H NMR spectra of **2** in d_6-DMSO: H_2O (1:1) solution, recorded at 0 and 72 hours respectively.

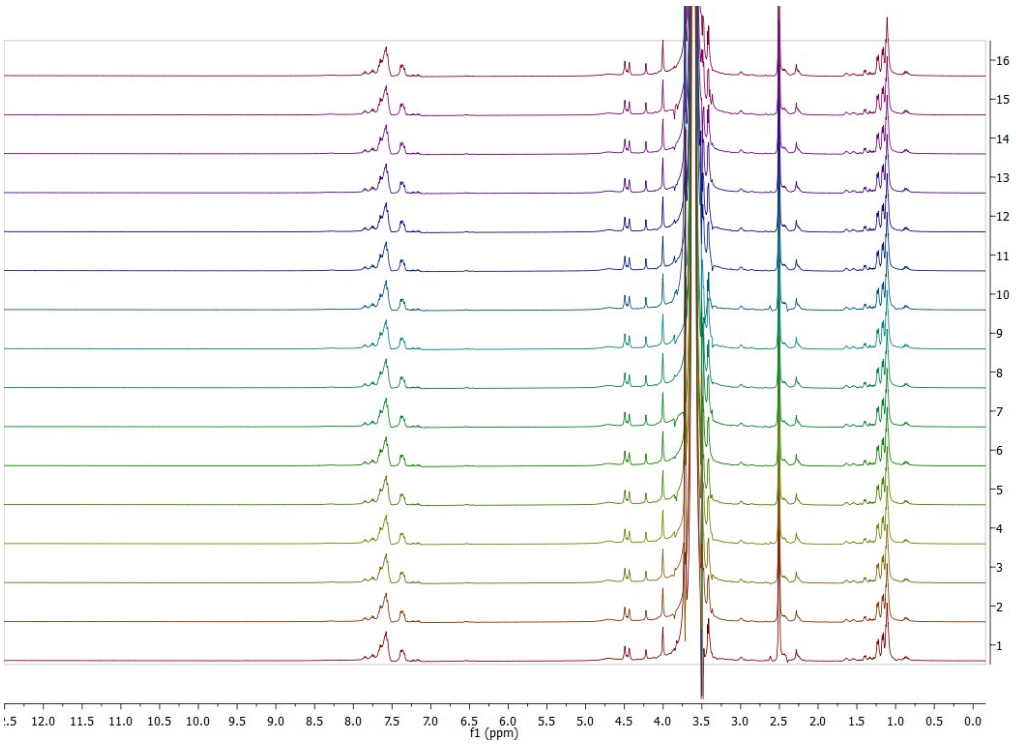

Figure **S17**. ^{1}H NMR spectra of **5** in d_6-DMSO: H_2O (1:1) solution, recorded over 180 min time intervals, over a total period of 48 h.

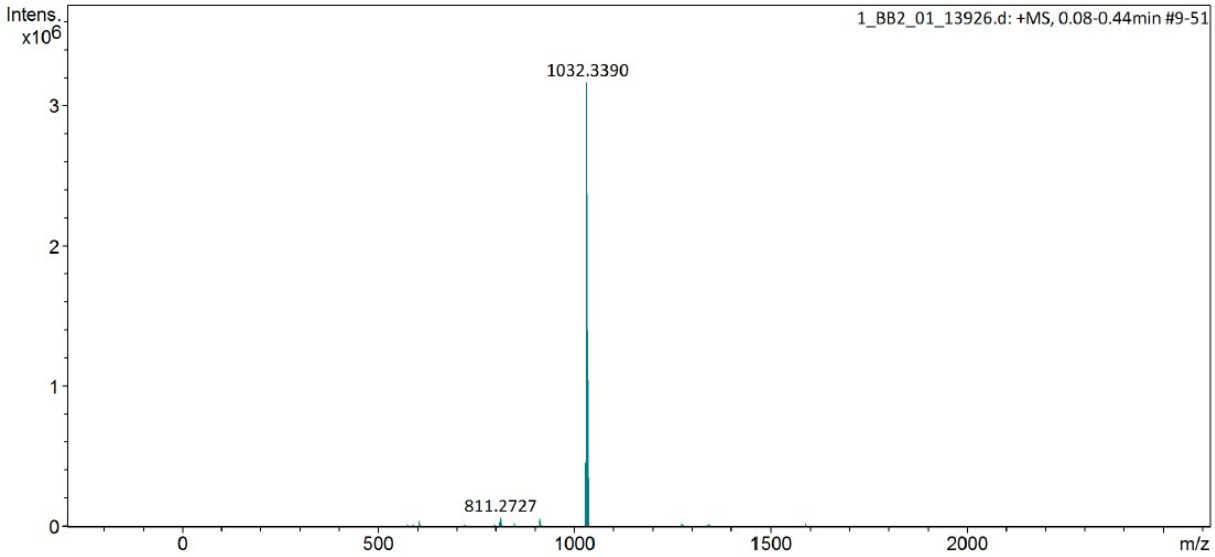

Figure **S18**. HRMS spectrum of **5** stored in DMSO at room temperature after 5 days.

V. Preliminary cytotoxicity screening of ligand salts **A**, **B** and complexes **2**–**6**

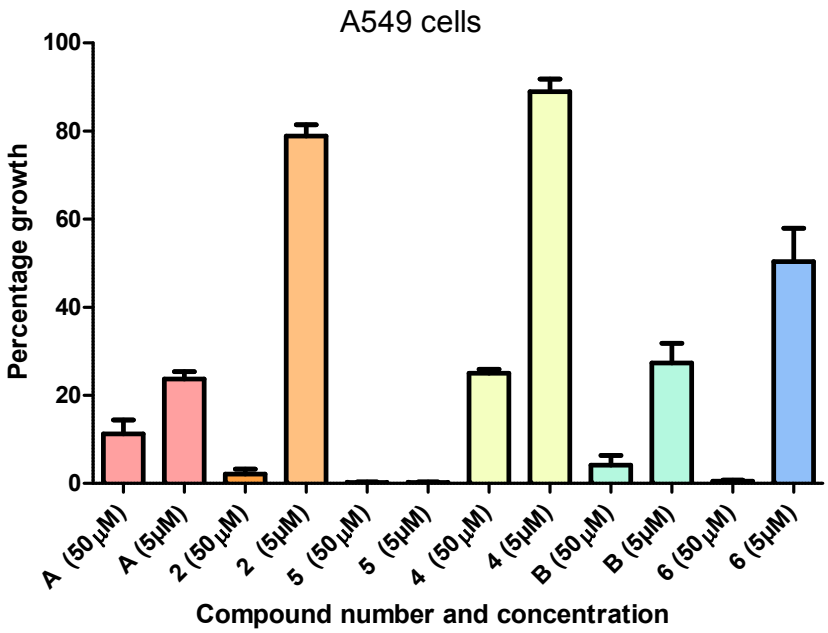

Figure **S19**. The percentage cell growth of A549 cells screened against ligand salts **A**, **B** and metal complexes **2**–**6** at 5 μM and 50 μM.

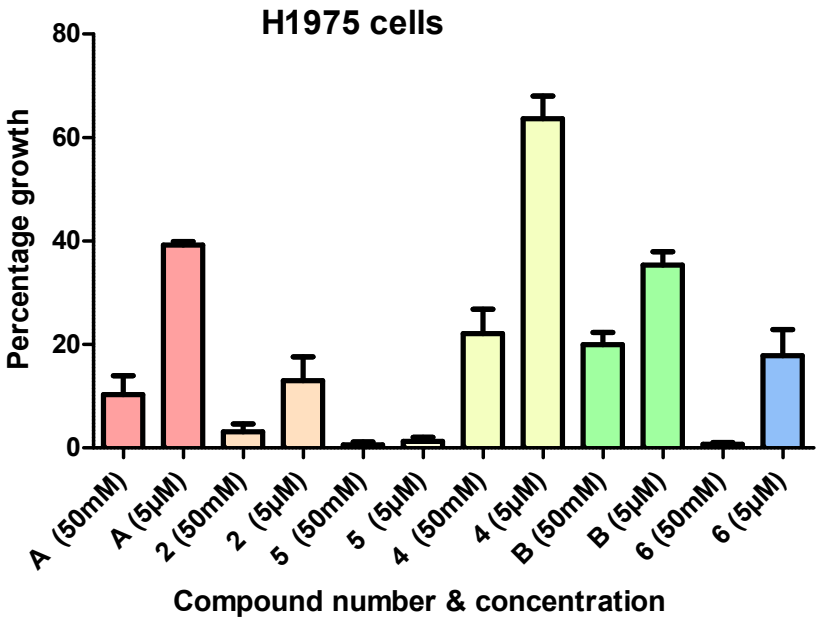

Figure **S20**. The percentage cell growth of H1975 cells screened against ligand salts **A**, **B** and metal complexes **2**–**6** at 5 μM and 50 μM.

VI. Fluorescence microscopy study on A549 cell line treated with **5**

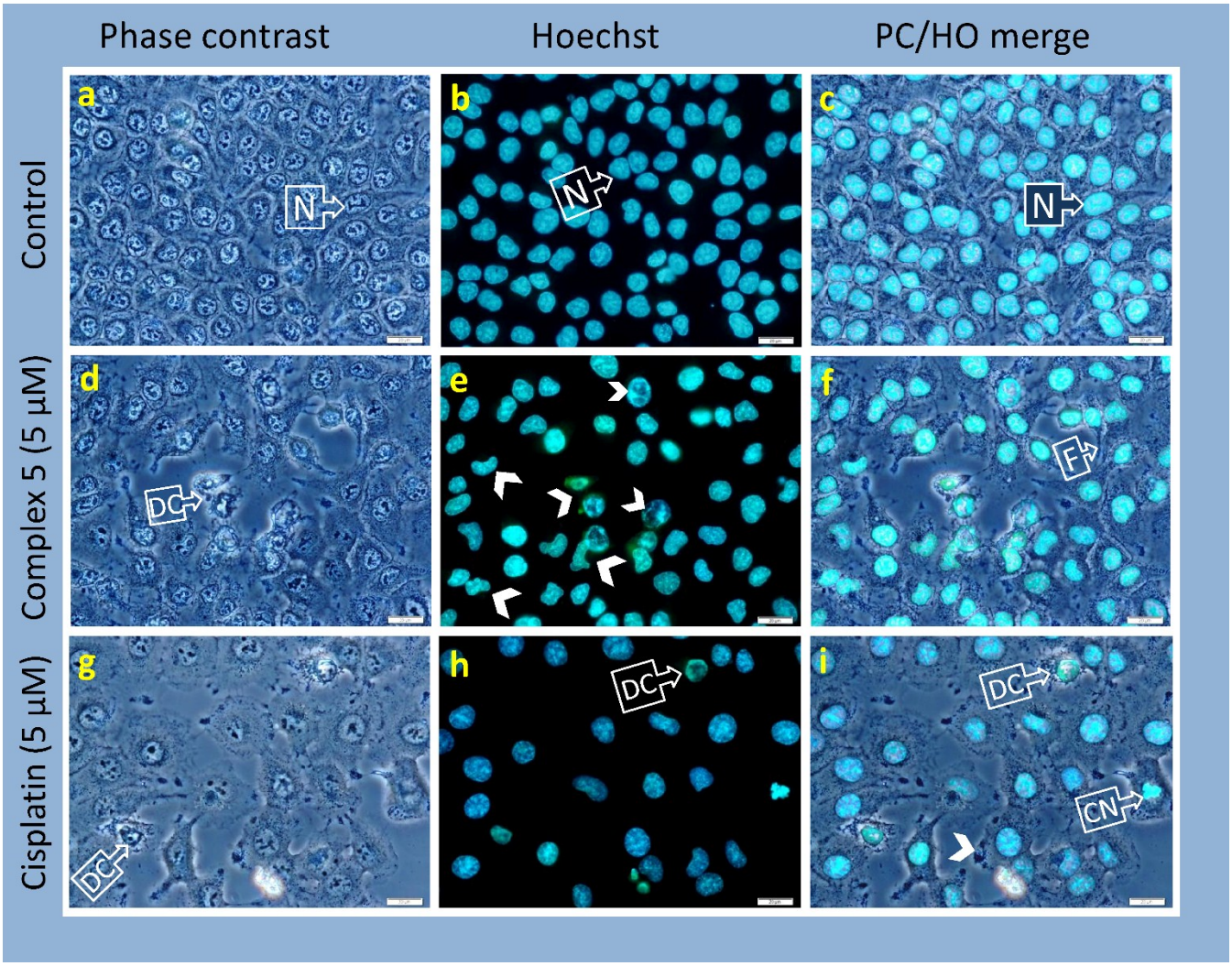

Figure. **S21**. A549 cells were treated with **5** at a concentration of 5 µM for 18 hours. Cells show a change in nuclear morphology and the absence of necrosis. Staining the live unfixed cells with Hoechst and ethidium bromide shows the absence of necrosis and changes in nuclear morphology as indicated in e and f, rounding of cells and the formation of filopodia. Cells were viewed under 400 X magnification with an Olympus BX41 epifluorescence microscope and images were captured with an Olympus DP72 digital camera and processed using the Olympus CellSens software package.

Scalebar: 20 microns. Legend: N=nucleus, DC= detached cell, F=filopodia, CN=contracted nucleus

Untreated A549 cells typically have an oval nucleus; when treated with **5** there was a change in the shape of many nuclei as indicated by the arrows (Fig. S19, panel e). Although the cells appeared to be intact (Fig. S19, panel d) many nuclei lost their typical ovioid shape. Changes to the normal nuclear morphology is followed by cell death. Filopodia were also visible in the cells that were affected by **5**. Cisplatin treated cells were more granular (indicated by the arrow in Figure S19 panel i) than untreated cells and the cell density was decreased when compared to the control cells.

VII. Crystal Structure Data for complexes **2**–**6**

*Crystal data for **2***

$C_{36}H_{43}AuClFeN_3$ (M = 806.00 g/mol): triclinic, space group P-1, a = 12.4522(10) Å, b = 12.5760(9) Å, c = 13.8786(8) Å, α = 116.729(2)°, β = 95.812(2) °, γ = 106.593(2)°, V = 1792.1(2) Å^3, Z = 2, T = 150 K, D_{calc} = 1.494 g/cm^3, μ(MoKα) = 4.594 mm^{-1}, 75451 reflections measured (2.36° ≤ 2Θ ≤ 28.28°), 8886 unique [R_{int} = 0.0848, R_{sigma} = 0.0530] which were used in all calculations. The final R_1 was 0.0342 (I > 2σ(I)) and wR_2 was 0.0665 (all data).

*Crystal data for **3***

$C_{42}H_{48}AuFeN_3$ (M = 847.65 g/mol): monoclinic, space group $P2_1/n$, a = 10.7939(19) Å, b = 22.047(4) Å, c = 15.733(3) Å, α = 90 °, β = 90.785(7) °, γ = 90 °, V = 3743.8(12) Å^3, Z = 4, T = 150 K, D_{calc} = 1.504 g/cm^3, μ(MoKα) = 4.334 mm^{-1}, 136890 reflections measured (4.548° ≤ 2Θ ≤ 54.496°), 8341 unique [R_{int} = 0.0490, R_{sigma} = 0.0183] which were used in all calculations. The final R_1 was 0.0210 (I > 2σ(I)) and wR_2 was 0.0500 (all data).

*Crystal data for **4***

$C_{73}H_{88}AgCl_2F_6Fe_2N_6P$ (M = 1484.93 g/mol): triclinic, space group P-1, a = 10.6222(5) Å, b = 15.5756(8) Å, c = 22.4569(10) Å, α = 84.938(3) °, β = 82.430(2) °, γ = 73.391(2) °, V = 3524.2(3) Å^3, Z = 2, T = 150 K, D_{calc} = 1.399 g/cm^3, μ(MoKα) = 0.841 mm^{-1}, 187604 reflections measured (4.192° ≤ 2Θ ≤ 66.458°), 27000 unique [R_{int} = 0.0445, R_{sigma} = 0.0315] which were used in all calculations. The final R_1 was 0.0374 (I > 2σ(I)) and wR_2 was 0.0921 (all data).

*Crystal data for **5***

$C_{55}H_{59}AuCl_3F_6FeN_3P_2$ (M = 1298.16 g/mol): monoclinic, space group $P2_1/c$, a = 17.8411(8) Å, b = 11.8539(6) Å, c = 26.3035(13) Å, α = 90 °, β = 97.359(2) °, γ = 90 °, V = 5517.0(5) Å^3, Z = 4, T = 150 K, D_{calc} = 1.563 g/cm^3, μ(MoKα) = 3.182 mm^{-1}, 221967 reflections measured (4.524° ≤ 2Θ ≤ 57.852°), 14373 unique [R_{int} = 0.0522, R_{sigma} = 0.0222] which were used in all calculations. The final R_1 was 0.0244 (I > 2σ(I)) and wR_2 was 0.0523 (all data).

*Crystal data for **6***

$C_{50}H_{54}AuF_6N_3P_2$ (M = 1069.87 g/mol): monoclinic, space group $P2_1/n$, a = 12.2845(10) Å, b = 34.873(3) Å, c = 22.3896(17) Å, α = 90 °, β = 101.251(2) °, γ = 90 °, V = 9407.3(13) Å^3, Z = 8, T = 173 K, D_{calc} = 1.511 g/cm^3, μ(MoKα) = 3.257 mm^{-1}, 190094 reflections measured (5.708° ≤ 2Θ ≤ 56.794°), 23549 unique [R_{int} = 0.0469, R_{sigma} = 0.0317] which were used in all calculations. The final R_1 was 0.0677 (I > 2σ(I)) and wR_2 was 0.1448 (all data).

VIII. References

1. APEX3, (including SAINT and SADABS), BrukerAXS Inc., Madison, WI, 2017.; G. M. Sheldrick, Acta Crystallogr., Sect. A: Found. Crystallogr., 2015, 71, 3–8.; G. M. Sheldrick, Acta Crystallogr., Sect. C: Cryst. Struct. Commun., 2015, 71, 3–8.; O.V. Dolomanov, L.J. Bourhis, R.J. Gildea, J.A.K. Howard, H. Puschmann, J. Appl. Cryst., 2009, 42, 339-341.